Reaction between Peroxynitrite and Boronates: EPR Spin-Trapping, HPLC Analyses, and Quantum Mechanical Study of the Free Radical Pathway

ARTICLE *in* CHEMICAL RESEARCH IN TOXICOLOGY · MARCH 2011

Impact Factor: 3.53 · DOI: 10.1021/tx100439a · Source: PubMed

7 AUTHORS, INCLUDING:

Adam Sikora
Lodz University of Technology
40 PUBLICATIONS **406** CITATIONS
SEE PROFILE

Jacek Zielonka
Medical College of Wisconsin
112 PUBLICATIONS **1,890** CITATIONS
SEE PROFILE

Marcos Lopez
Fundación Cardiovascular de Colombia
25 PUBLICATIONS **831** CITATIONS
SEE PROFILE

Agnieszka Dybala-Defratyka
Lodz University of Technology
36 PUBLICATIONS **342** CITATIONS
SEE PROFILE

Chemical Research in Toxicology

ARTICLE

pubs.acs.org/crt

Reaction between Peroxynitrite and Boronates: EPR Spin-Trapping, HPLC Analyses, and Quantum Mechanical Study of the Free Radical Pathway

Adam Sikora,[†,‡] Jacek Zielonka,[†] Marcos Lopez,[†] Agnieszka Dybala-Defratyka,[‡] Joy Joseph,[†] Andrzej Marcinek,[‡] and Balaraman Kalyanaraman*[,†]

[†]Department of Biophysics and Free Radical Research Center, Medical College of Wisconsin, Milwaukee, Wisconsin, United States

[‡]Institute of Applied Radiation Chemistry, Technical University of Lodz, Poland

Supporting Information

ABSTRACT: Recently, we showed that peroxynitrite ($ONOO^-$) reacts directly and rapidly with aromatic and aliphatic boronic acids ($k \approx 10^6\ M^{-1}s^{-1}$). Product analyses and substrate consumption data indicated that $ONOO^-$ reacts stoichiometrically with boronates, yielding the corresponding phenols as the major product (~85−90%), and the remaining products (10−15%) were proposed to originate from free radical intermediates (phenyl and phenoxyl radicals). Here, we investigated in detail the minor, free radical pathway of boronate reaction with $ONOO^-$. The electron paramagnetic resonance (EPR) spin-trapping technique was used to characterize the free radical intermediates formed from the reaction between boronates and $ONOO^-$. Using 2-methyl-2-nitrosopropane (MNP) and 5-diethoxyphosphoryl-5-methyl-1-pyrroline-*N*-oxide (DEPMPO) spin traps, phenyl radicals were trapped and detected. Although phenoxyl radicals were not detected, the positive effects of molecular oxygen, and inhibitory effects of hydrogen atom donors (acetonitrile, and 2-propanol) and general radical scavengers (GSH, NADH, ascorbic acid, and tyrosine) on the formation of phenoxyl radical-derived nitrated product, suggest that the phenoxyl radical was formed as the secondary species. We propose that the initial step of the reaction involves the addition of $ONOO^-$ to the boron atom in boronates. The anionic intermediate undergoes both heterolytic (major pathway) and homolytic (minor pathway) cleavage of the peroxy (O−O) bond to form phenol and nitrite as a major product (via a nonradical mechanism), or a radical pair $PhB(OH)_2O^{\bullet-}\cdots{}^{\bullet}NO_2$ as a minor product. It is conceivable that phenyl radicals are formed by the fragmentation of the $PhB(OH)_2O^{\bullet-}$ radical anion. According to the DFT quantum mechanical calculations, the energy barrier for the dissociation of $PhB(OH)_2O^{\bullet-}$ radical anion to form phenyl radical is only a few kcal/mol, suggesting rapid and spontaneous fragmentation of the $PhB(OH)_2O^{\bullet-}$ radical anion in aqueous media. Biological implications of the minor free radical pathway are discussed in the context of $ONOO^-$ detection, using the boronate probes.

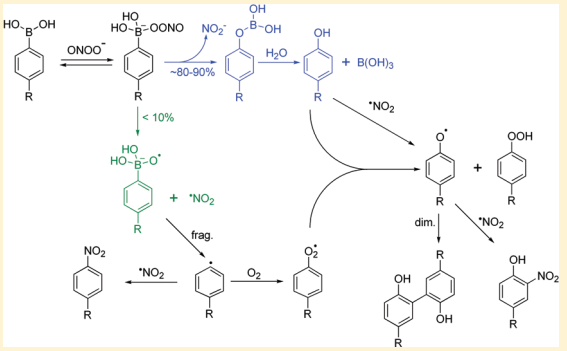

INTRODUCTION

Peroxynitrite ($ONOO^-/ONOOH$), a potent biological oxidizing and nitrating agent, is formed from a diffusion-controlled reaction between nitric oxide ($^{\bullet}NO$) and superoxide radical anion ($O_2^{\bullet-}$).[1−3] Under pathophysiological conditions, the rate of formation of $ONOO^-$ is enhanced due to higher rates of $O_2^{\bullet-}$ and/or $^{\bullet}NO$ generation.[4] $ONOO^-$ has been implicated in a variety of disease states, including cardiovascular, neurodegenerative, and inflammatory disorders.[4,5] Recently, we showed that phenyl and coumarin boronates react with $ONOO^-$ rapidly ($k \sim 10^6\ M^{-1}s^{-1}$ at pH 7.4) and stoichiometrically, yielding the corresponding phenols as the major products (85−90%).[6,7] In addition, a few minor products presumably derived from free radical intermediates (phenyl and phenoxyl radicals) were detected (Scheme 1). Boronate-based fluorescent detection of $ONOO^-$ is likely to become a routine methodology in redox biology.[6−9]

The present study is focused on the identification of free radical intermediates formed during the reaction of boronates with $ONOO^-$. $ONOO^-$ was added as a bolus or generated *in situ* under equal or different fluxes of $^{\bullet}NO$ and $O_2^{\bullet-}$.[6,7] For the EPR spin trapping experiment, both MNP (2-methyl-2-nitrosopropane) and 5-diethoxyphosphoryl-5-methyl-1-pyrroline-*N*-oxide (DEPMPO) were used as spin traps.[10,11] The effects of oxygen and radical scavengers (GSH, NADH, ascorbic acid, tyrosine, and 2-propanol) on the yields and distribution of the minor products were examined. Results from the spin-trapping experiments and

Received: December 17, 2010
Published: March 24, 2011

Scheme 1. Oxidation of Boronic Acids by Peroxynitrite: Major and Minor Oxidation Products and Postulated Radical Intermediates

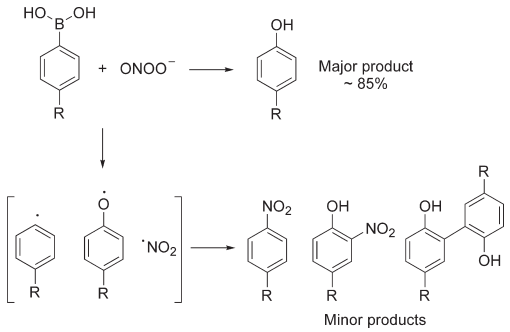

product analyses strongly suggest a mechanism of the minor, free radical pathway (yield <15%) of the reaction of $ONOO^-$ with boronates. We propose a mechanism involving a homolytic cleavage of the O−O bond of the $ONOO^-$ adduct to the boronate group with the formation of a caged radical pair $[PhB(OH)_2O^{\bullet-}\cdots\cdots{}^{\bullet}NO_2]$ and subsequent formation of phenyl radical species.

EXPERIMENTAL PROCEDURES

Chemicals. Phenylalanine-4-boronic acid (FBA) was obtained from Ryscor Science (Wake Forest, NC), and other boronates were purchased from Boron Molecular (Research Triangle, NC). MNP was obtained from Sigma-Aldrich Corp. (St. Louis, MO), and DEPMPO was obtained from Radical Vision (Marseille, France). All other reagents (of highest purity available) were from Sigma-Aldrich Corp. All solutions were prepared using deionized water (Millipore Milli-Q system). $ONOO^-$ was prepared by reacting nitrite with H_2O_2, according to the published procedure.[12] The concentration of $ONOO^-$ in alkaline aqueous solutions (pH > 12) was determined by measuring the absorbance at 302 nm (ε = 1670 $M^{-1}cm^{-1}$).[12] PAPA-NONOate [13,14] was from Cayman Chemical Company (Ann Arbor, MI). Xanthine oxidase (XO), superoxide dismutase (SOD), and catalase were obtained from Roche Applied Science (Indianapolis, IN).

Determination of $O_2^{\bullet-}$ and $^{\bullet}NO$ Fluxes. $^{\bullet}NO$ fluxes were determined from the measured rate of the decomposition of PAPA-NONOate by following the decrease in its characteristic absorbance at 250 nm ($\varepsilon = 8 \times 10^3$ M^{-1} cm^{-1}).[13,14] This rate was multiplied by a factor of 2 to obtain the rate of $^{\bullet}NO$ release (assuming that two molecules of $^{\bullet}NO$ are released from one molecule of PAPA-NONOate). The flux of $O_2^{\bullet-}$ was determined by monitoring the cytochrome *c* reduction following the increase in absorbance at 550 nm (using an extinction coefficient of 2.1 × 10^4 $M^{-1}cm^{-1}$).[15]

HPLC Analyses of Oxidation Products. 4-Acetylphenylboronic acid (APBA), 4-hydroxyacetophenone (HAP), 4-hydroxy-3-nitroacetophenone (HNAP), 4-nitroacetophenone (NAP), and acetophenone (AP) were separated on an Agilent 1100 HPLC system equipped with fluorescence and UV−vis absorption detectors.[6] Typically, 100 μL of sample was injected into the HPLC system equipped with a C_{18} column (Alltech, Kromasil, 250 mm × 4.6 mm, 5 μm) equilibrated with 5% CH_3CN [containing 0.1% (v/v) trifluoroacetic acid (TFA)] in 0.1% TFA aqueous solution. The compounds were separated by a linear increase in CH_3CN phase concentration from 5 to 100% over 30 min, using a flow rate of 1 mL/min. Under those conditions APBA eluted at 10.7 min, HAP at 11.3 min, HNAP at 14.9 min, AP at 15.7 min, and NAP at 16.7 min. The peak areas detected by monitoring the absorption at 252 nm (APBA, HNAP, and HP), 274 nm (HAP), and 266 nm (NAP) were used in the quantitation.

UV−Vis Absorption and Fluorescence Measurements. The UV−vis absorption spectra were collected using an Agilent 8453 spectrophotometer equipped with a diode array detector and thermostated cell holder. Fluorescence spectra were collected at room temperature using the Perkin-Elmer LS 55 luminescence spectrometer.

EPR Spin-Trapping Experiments. Typically, incubation mixtures used in spin-trapping experiments consisted of boronic acids (50−250 μM) and MNP (20 mM) or DEPMPO (20 mM) in a phosphate buffer (50 mM, pH 7.4) containing DTPA (100 μM) and were rapidly mixed with bolus $ONOO^-$ (50−250 μM) or with cogenerated $^{\bullet}NO$ and $O_2^{\bullet-}$.[7] For experiments with *in situ* generation of $^{\bullet}NO$ and $O_2^{\bullet-}$, boronic compounds (250 μM) were incubated with XO (generating the flux of $O_2^{\bullet-}$ of 6 μM/min), xanthine (X) (200 μM), and PAPA-NONOate (generating the appropriate flux of $^{\bullet}NO$ in the range of 1.5−24 μM/min) in phosphate buffer (50 mM, pH 7.4) containing DTPA (100 μM) at room temperature for 5 min. Reaction mixtures contained catalase (200 U/mL) and/or superoxide dismutase (SOD) enzyme (0.05 mg/mL), where indicated. Samples were subsequently transferred to an EPR cell, and spectra were taken in a Bruker EMX spectrometer. Typical spectrometer parameters were as follows: scan range, 150 G; field set, 3470 G; time constant, 1.28 ms; scan time, 84 s; modulation amplitude, 1.0 G; modulation frequency, 100 kHz; receiver gain, 1 × 10^5; and microwave power, 20 mW. The spectra shown were the average of 5 scans.

For the quantitative analysis, the MNP-acetylphenyl radical adduct was generated in incubations containing the following components: APBA (250 μM), peroxynitrite (50, 100, 150, 200 μM), and MNP (20 mM) in a phosphate buffer (50 mM, pH 7.4) containing DTPA (100 μM). The reaction mixture was transferred to an EPR cell immediately after mixing with peroxynitrite, and spectra were immediately recorded. Tempol was used as a calibration standard, and its concentration was determined using the extinction coefficient of 1440 $M^{-1}cm^{-1}$ at 240 nm. The yield of the MNP-acetylphenyl radical adduct was calculated by a comparison of the double integral of the spectra of a known concentration of Tempol with the slope coefficient of the linear dependence of the double integrals of the spectra of the MNP-acetylphenyl radical adduct on the concentration of added peroxynitrite.

Theoretical Studies. All calculations were done using the Gaussian 09 rev.A.02 (G09) package.[16] Geometries and energies were calculated using the M06-2X functional of Truhlar and co-workers, recently developed and parametrized for thermochemical kinetics and noncovalent interactions[17,18] with the 6-31+G(d,p) basis set.[19,20] Initial geometry of the $PhB(OH)_2O^{\bullet-}$ radical anion was fully optimized and used for the relaxed potential energy scan performed along the reaction coordinate defined as an elongating boron−carbon bond length. All structures on the potential energy surfaces were fully optimized, and the stationary points were confirmed by performing harmonic vibrational analysis. Local minima were characterized by 3N-6 real normal modes of vibrations, whereas the transition states had exactly one imaginary frequency. The influence of the environment was modeled using the polarizable continuum solvent model (PCM)[21] with parameters for water as implemented in G09; only the electrostatic effects were included in the continuum solvent model calculations. Open shell species were treated using the unrestricted Hartree−Fock (UHF) method.[22] We have used the default convergence and optimization criteria in all calculations performed using the Gaussian package.

RESULTS

EPR Spin-Trapping of Phenyl Radicals. The EPR spin-trapping studies with MNP and DEPMPO were carried out to detect and characterize radical intermediates during the reaction of $ONOO^-$ with boronates. The addition of a bolus amount of $ONOO^-$ to incubations containing APBA and MNP (pH 7.4) yielded a multiline spectrum [a_N = 13.40 G; a_H = 2.06 G (2H);

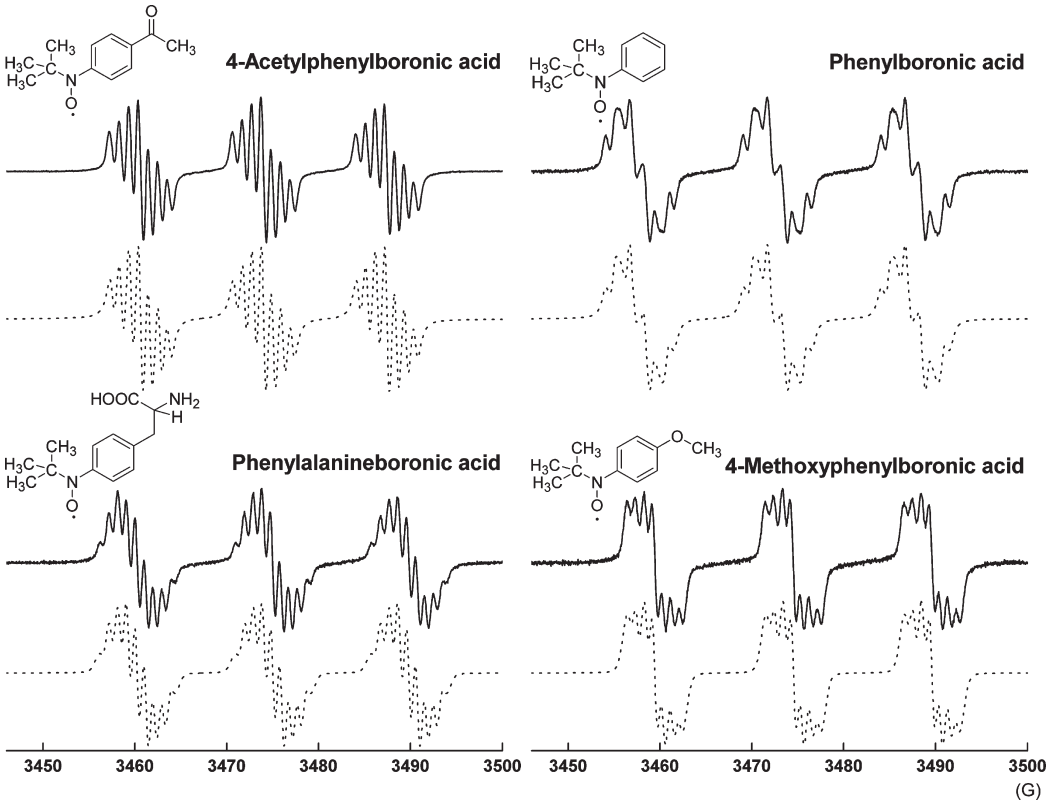

Figure 1. Spin-trapping of phenyl radicals formed from the reaction between $ONOO^-$ and selected phenylboronic acids. Incubation mixtures contained the following components: phenylboronic acid (250 μM), $ONOO^-$ (250 μM), and MNP (20 mM) in a phosphate buffer (100 mM, pH 7.4) containing DTPA (100 μM). The reaction mixture was transferred to an EPR flat cell immediately after adding a bolus amount of $ONOO^-$, and spectra were recorded at room temperature. Solid and dotted lines represent experimental and simulated spectra, respectively.

Table 1. Hyperfine Coupling Constants of DEPMPO and MNP Spin Adducts

	hyperfine splitting constants [G]
MNP	
phenylboronic acid	a_N = 14.98; a_{ortho}(2H) = 1.61; a_{para}(1H) = 1.51; a_{meta}(2H) = 0.96
4-methoxyphenylboronic acid	a_N = 15.06; a_{ortho}(2H) = 1.85; a_{meta}(2H) = 0.89
4-acetylphenylboronic acid	a_N = 13.40; a_{ortho}(2H) = 2.06; a_{meta}(2H) = 0.99
phenylalanineboronic acid	a_N = 14.77; a_{ortho}(2H) = 1.90; a_{meta}(2H) = 1.00
DEPMPO	
4-acetylphenylboronic acid	a_N = 14.68; a_H = 22.85; a_P = 44.86
$GS^•$ radical	a_N = 14.16; a_H = 14.93; a_P = 46.13

a_H = 0.99 G (2H)] (Figure 1), which was assigned to the MNP-acetylphenyl radical adduct. Incubation of $ONOO^-$ with phenylalanine-4-boronic, phenylboronic, and 4-methoxyphenylboronic acids also led to multiline EPR spectra which were assigned to their corresponding MNP-phenyl radical adducts based on the hyperfine coupling values (Table 1).[23] The spectral intensity of MNP-phenyl radical adducts increased with increasing boronate and $ONOO^-$ concentrations (Figure 2).

The addition of $ONOO^-$ to incubations containing boronate and DEPMPO in phosphate buffer (pH 7.4, 100 mM) yielded a 12-line EPR spectrum attributable to a DEPMPO-carbon centered adduct with the unpaired electron interacting with a hydrogen, nitrogen, and phosphorus nuclei (Figure 3).[11,24] On the basis of the values of hyperfine coupling constants (Table 1), the DEPMPO spectrum was assigned to the DEPMPO-phenyl radical adduct.[25] As with MNP, the intensities of the DEPMPO-phenyl radical adduct increased with increasing boronate and $ONOO^-$ concentrations (Figure 3). These results suggest that phenyl radicals are formed in a direct bimolecular reaction between boronates and peroxynitrite. Although we were unable to detect the spin adduct of the phenoxyl radical, the EPR spin-trapping results strongly suggest that phenyl-type radicals are formed from the decomposition of the intermediate formed from the arylboronates/$ONOO^-$ interaction.

To investigate whether the same EPR signals of the phenyl radical adduct to the spin trap can be observed during the reaction between boronates and peroxynitrite formed from cogenerated superoxide and nitric oxide, the oxidation of APBA was investigated in the X/XO/PAPA-NONOate system. APBA (250 μM) was incubated with X (200 μM) and XO (generating the flux of $O_2^{•-}$ of 6 μM/min) in phosphate buffer (50 mM, pH 7.4) containing DEPMPO (20 mM) and PAPA-NONOate (200 μM that released $^•NO$ flux of 6 μM/min). Similar incubations were also performed in the presence of SOD (0.05 mg/mL). Figure 4 (left panel) shows the EPR spectra obtained from incubations in the absence of SOD. The spectrum of the superoxide radical adduct of DEPMPO (DEPMPO-OOH) obtained from incubations containing X/XO was replaced by the spectrum of the hydroxyl radical adduct of DEPMPO (DEPMPO-OH) in

dx.doi.org/10.1021/tx100439a |*Chem. Res. Toxicol.* 2011, 24, 687–697

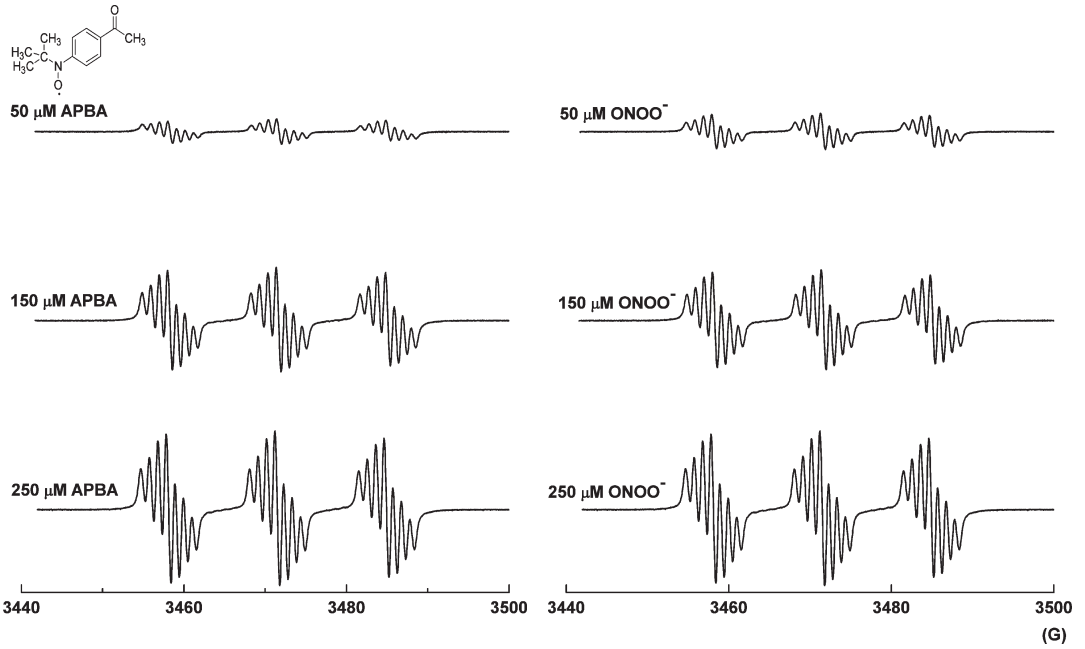

Figure 2. Dose-dependent increase in spin adduct formation: Effects of varying $ONOO^-$ and acetylphenylboronic acid. (Left panel) Incubation mixtures contained the following components: APBA (50, 150, 250 μM), $ONOO^-$ (250 μM), and MNP (20 mM) in a phosphate buffer (100 mM, pH 7.4) containing DTPA (100 μM). The reaction mixture was transferred to an EPR cell immediately after adding the peroxynitrite by the bolus addition to the other components, and spectra were recorded at room temperature. (Right panel) Incubation conditions were the same as above except that APBA was used at a concentration of 250 μM, and the concentration of $ONOO^-$ was varied (50, 150, 250 μM). Other experimental conditions are as indicated.

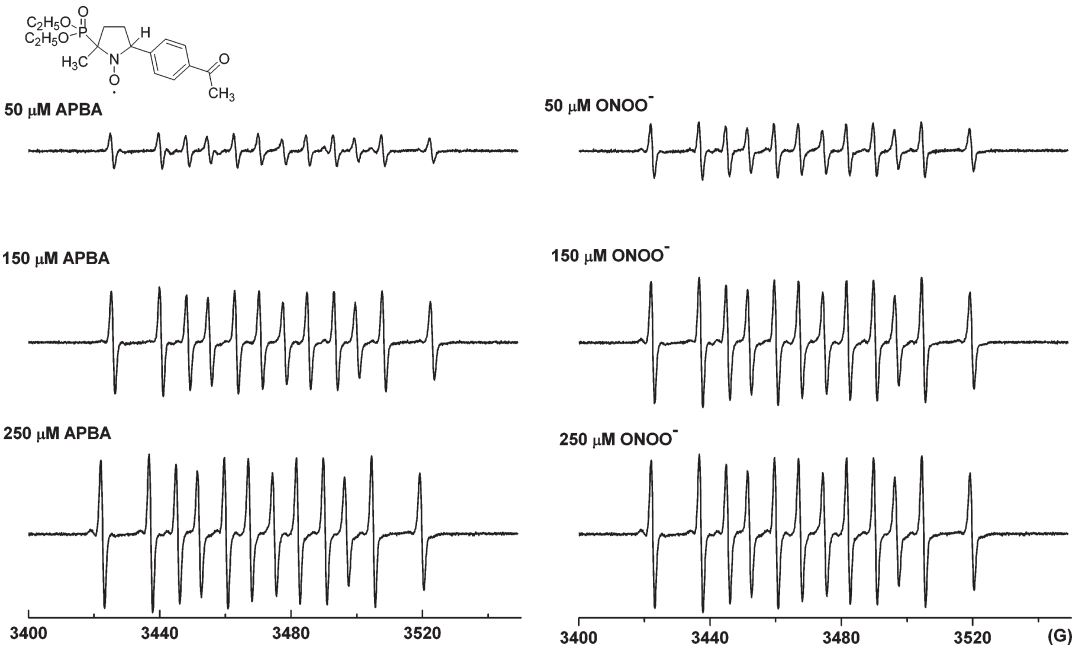

Figure 3. DEPMPO spin-trapping of the acetylphenyl radical formed from a reaction between $ONOO^-$and acetylphenylboronic acid. (Left panel) Incubation mixtures contained the following components: APBA (50, 150, 250 μM), $ONOO^-$ (250 μM), and DEPMPO (20 mM) in a phosphate buffer (100 mM, pH 7.4) containing DTPA (100 μM). The reaction mixture was transferred to an EPR cell immediately after adding the peroxynitrite by the bolus addition to the other components, and spectra were recorded at room temperature. (Right panel) Incubation conditions were the same as above except that APBA was used at concentration of 250 μM, and the concentration of $ONOO^-$ was varied (50, 150, 250 μM). Other experimental conditions are as indicated.

the presence of PAPA-NONOate, and by the phenyl radical adduct of DEPMPO (DEPMPO-Ph) in the presence of PAPA-NONOate and APBA (Figure 4, left panel). These spectral changes are attributed to the trapping of hydroxyl radicals (formed from the decomposition of $ONOO^-$) and phenyl radicals (formed from the decomposition of the APBA/$ONOO^-$ adduct) by DEPMPO. In the absence of PAPA-NONOate, boronate reduced the DEPMPO-OOH adduct to the

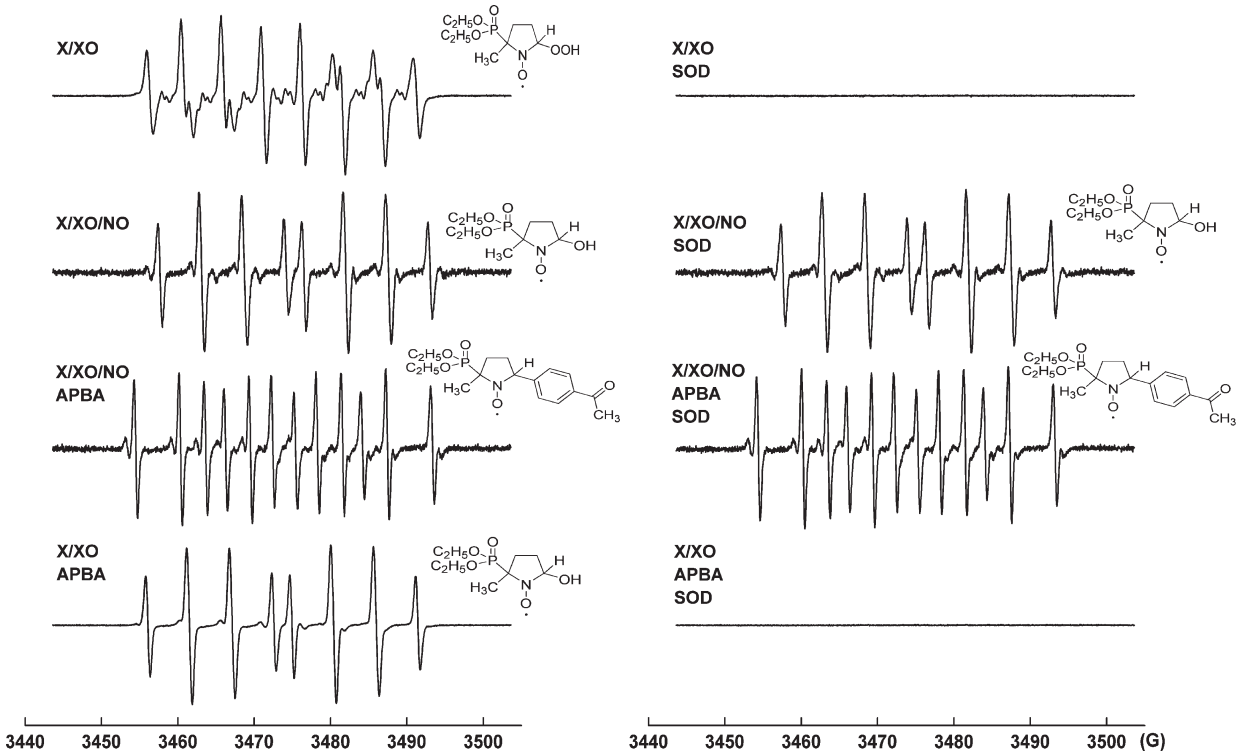

Figure 4. DEPMPO spin-trapping of radicals formed from the reaction between acetylphenylboronic acid and cogenerated $^{\bullet}NO$ and $O_2^{\bullet-}$. (Left panel) Incubation mixtures containing xanthine (X, 200 μM), xanthine oxidase (XO, generating a flux of $O_2^{\bullet-}$ of 6 μM/min), PAPA-NONOate (generating a flux of $^{\bullet}NO$ of 6 μM/min), APBA (250 μM), and DEPMPO (20 mM) in a phosphate buffer (50 mM, pH 7.4) containing DTPA (100 μM). The reaction mixture was transferred to an EPR cell immediately after mixing, and spectra were recorded at room temperature after incubation for 5 min. (Right panel) The same as the left panel, but in the presence of SOD (0.05 mg/mL).

DEPMPO-OH. Using the coumarin boronate, we determined the rate constant for the coumarin boronate-mediated reduction of the DEPMPO-OOH adduct to the DEPMPO-OH adduct to be ca. 39 $M^{-1}s^{-1}$ (Supporting Information, Figure S1). During this reaction, coumarin boronate was converted to hydroxycoumarin, which was monitored using the fluorescence detection method.[7]

In parallel, we investigated the effect of SOD on DEPMPO spin adduct formation (Figure 4, right panel). At the concentrations used, SOD abolished the formation of DEPMPO-OOH and DEPMPO-OH formed from incubations containing X/XO and APBA but did not affect the formation of the DEPMPO-Ph adduct detected in the presence of X/XO, APBA, and PAPA-NONOate. These results are consistent with the rapid reaction between $^{\bullet}NO$ and $O_2^{\bullet-}$ as compared to the SOD-catalyzed dismutation of $O_2^{\bullet-}$.

We then monitored the effect of variation of $^{\bullet}NO/O_2^{\bullet-}$ flux ratios on the DEPMPO-Ph adduct yields. Spin trapping experiments were performed in incubation mixtures containing DEPMPO, APBA, a constant flux of $O_2^{\bullet-}$ (6 μM/min), and different fluxes of $^{\bullet}NO$ (0−24 μM/min) obtained by varying the concentrations of PAPA-NONOate (0−770 μM). Figure 5 (left panel) shows the DEPMPO spin adduct spectra formed from incubations containing SOD. As shown, as the $^{\bullet}NO/O_2^{\bullet-}$ flux ratio varied from 1:4 to 4:1, the EPR signal intensity of the DEPMPO-Ph spin adduct increased until the $^{\bullet}NO/O_2^{\bullet-}$ ratio reached unity and later remained at the same level with increasing $^{\bullet}NO$. These results are attributed to the formation of $ONOO^-$ followed by a rapid reaction between APBA and $ONOO^-$ with the formation of phenyl radicals. Figure 5 (right panel) shows the DEPMPO spin adduct spectra formed from the same incubations in the absence of SOD. At low rates of $^{\bullet}NO$ generation ($^{\bullet}NO/O_2^{\bullet-}$ flux ratio of 1:4), the DEPMPO-OH spin adduct was predominant with considerably less contribution from the DEPMPO-Ph adduct. However, with increasing rates of $^{\bullet}NO$ generation, the intensity of the DEPMPO-Ph adduct became more intense, reaching a maximal level at equal rates of generation of $^{\bullet}NO$ and $O_2^{\bullet-}$.

Free Radical-Mediated Products of Boronate Reaction with Peroxynitrite. Although the reaction between boronates and $ONOO^-$ is stoichiometric, the hydroxyl derivative accounts for only 85−90% of the total amount of the consumed boronate. Previously, we reported that oxidation of phenylalanine boronic acid by peroxynitrite resulted in the formation of tyrosine as a major product and nitrotyrosine and dityrosine as minor products.[6] Moreover, nitrotyrosine and dityrosine were formed even in the presence of an excess of phenylalanine-4-boronic acid. Under these conditions, the probability of the reaction between $ONOO^-$ and the corresponding phenol (i.e., tyrosine) forming nitrotyrosine and dityrosine was negligible. We used the HPLC technique to monitor the profile of distribution of the minor products formed during the reaction between $ONOO^-$ and APBA. Figure 6 shows the HPLC chromatogram of the reaction between APBA (250 μM) and $ONOO^-$ (200 μM). In the presence of $ONOO^-$, the intensity of the peak due to APBA (eluting at 10.7 min) decreased, and additional peaks eluting at 11.3, 14.9, and 16.7 min emerged. These have been assigned to the major oxidation product 4′-hydroxyacetophenone (HAP, 11.3 min), 4′-hydroxy-3′-nitroacetophenone (HNAP, 14.9 min), and 4′-nitroacetophenone (NAP, 16.7 min) after comparing with

dx.doi.org/10.1021/tx100439a |*Chem. Res. Toxicol.* 2011, 24, 687–697

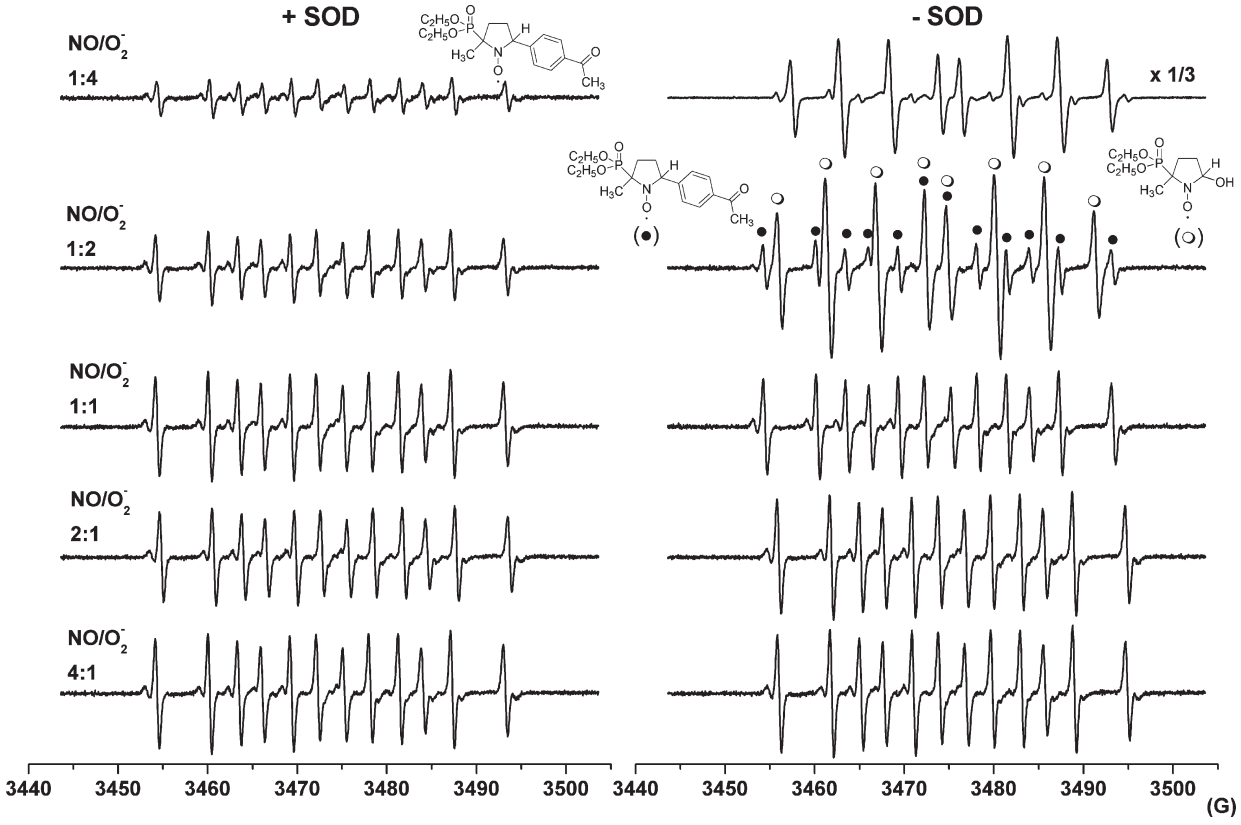

Figure 5. Effect of varying $^{\bullet}NO$ and $O_2^{\bullet-}$ flux on DEPMPO spin-trapping of radicals formed from acetylphenylboronic acid. (Left panel) Incubation mixtures contained the following components: xanthine (X, 200 μM), xanthine oxidase (XO, generating a flux of $O_2^{\bullet-}$ of 6 μM/min), PAPA-NONOate (generating a flux of $^{\bullet}NO$ yielding the $^{\bullet}NO/O_2^{\bullet-}$ ratios indicated above the traces), APBA (250 μM), and DEPMPO (20 mM) in a phosphate buffer (100 mM, pH 7.4) containing DTPA (100 μM) and SOD (0.05 mg/mL). (Right panel) Incubation conditions were the same as in the left panel except that SOD was omitted. The reaction mixture was transferred to an EPR cell immediately after mixing, and spectra were recorded at room temperature after incubation for 5 min.

the corresponding authentic standards. These results indicate that nitrogen dioxide ($^{\bullet}NO_2$), phenoxyl ($PhO^{\bullet}$), and phenyl ($Ph^{\bullet}$) radicals were formed during the oxidation of APBA by $ONOO^-$. As only the formation of the phenyl radical is supported by EPR experiments and quantum chemical calculations (see below), it is likely that the phenoxyl radical is formed as the secondary intermediate with respect to $Ph^{\bullet}$ and/or $^{\bullet}NO_2$ radicals. It is known that phenyl radicals react very rapidly with oxygen (the second order rate constant is about 10^9 $M^{-1}s^{-1}$)[26−30] with the formation of a highly oxidizing phenylperoxyl radical ($PhO_2^{\bullet}$) capable of oxidizing the phenolic compounds (the magnitude of second order rate constant depends on the phenol structure, but in many cases is in the range of 10^6 $M^{-1}s^{-1}$).[28−30] We surmised that if these reactions play a role in the formation of phenoxyl radical-derived products (i.e., HNAP), then their yields should depend on the oxygen concentration. Therefore, we investigated the effect of oxygen on the yield of nitration and oxidation products. Figure 7A and B show the effect of increasing concentrations of O_2 on HNAP, AP, and NAP formation in incubation mixtures containing APBA in phosphate buffer (pH 7.4, 50 mM) containing DTPA (100 μM). Enhanced formation of NAP and AP (phenyl radical-derived products), and decreased formation of HNAP (phenoxyl radical-derived product) were observed when incubations were deaerated by bubbling with argon gas. The decrease in the yield of NAP in the presence of oxygen may be explained in terms of the competition between $^{\bullet}NO_2$ and O_2 for the phenyl radical.

To determine whether other radical scavengers (phenyl radical scavengers, in particular) had any influence on the minor oxidation products' profiles, we investigated the effects of acetonitrile (MeCN), MNP (2-methyl-2-nitrosopropane), 2-PrOH (2-propanol), L-tyrosine, and ABTS (2,2′-azino-bis(3-ethylbenzothiazoline-6-sulfonate). Both $Ph^{\bullet}$ and $^{\bullet}NO_2$ radicals are formed together within the solvent cage where they can readily recombine to form NAP as a product or diffuse away to the bulk solvent. Acetonitrile is a poor radical scavenger, but it can serve as a H-atom donor under certain conditions, i.e., in the presence of highly reactive radicals (such as $^{\bullet}OH$ or $^{\bullet}H$) that are capable of abstracting a hydrogen atom.[31] As shown in Figure 8, the yield of AP was slightly enhanced and that of NAP was slightly decreased in the presence of 2.5% MeCN, suggesting that the radical formed is a good hydrogen atom acceptor. Reaction mixtures containing MeCN served as a control for the sample containing the MNP spin trap since MeCN was used as a solvent for MNP stock solutions. As shown in Figure 8, inclusion of MNP (20 mM) inhibited the formation of radical-derived products, AP and HNAP. In contrast to MeCN, 2-PrOH is a good hydrogen atom donor in reactions with radicals capable of abstracting H-atoms, and reacts with phenyl radicals rapidly ($k \sim 10^6-10^7$ $M^{-1}s^{-1}$).[28,30,32] As can be seen in Figure 8, the addition of 2-PrOH inhibited HNAP formation with a concomitant increase in the yield of AP, suggesting the direct scavenging of the $Ph^{\bullet}$ radical. ABTS is a potent radical scavenger that can be oxidized by many radical species to a stable radical cation

dx.doi.org/10.1021/tx100439a |Chem. Res. Toxicol. 2011, 24, 687–697

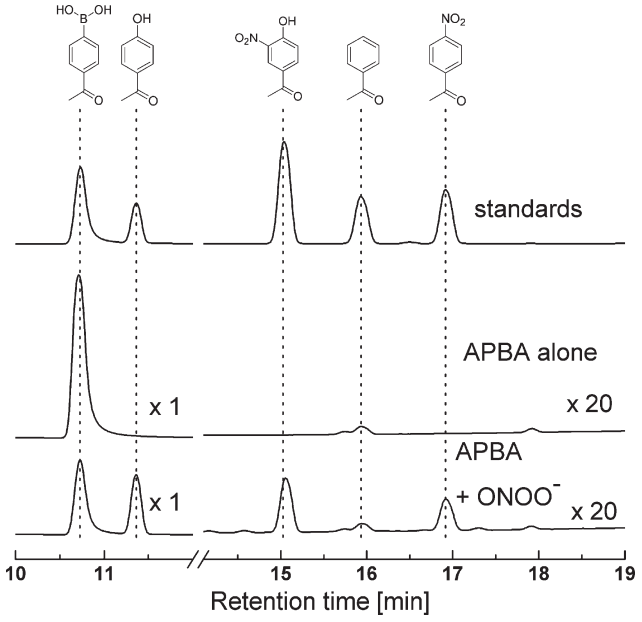

Figure 6. HPLC chromatograms of products formed from the reaction between acetylphenyl boronic acid and $ONOO^-$. (Upper trace) HPLC/UV (detection at 252 nm) analyses of standards of APBA, HAP, HNAP, AP, and NAP (100 μM), (middle trace) incubations containing APBA (250 μM) in phosphate buffer (pH 7.4, 100 mM) containing DTPA (10 μM), and (bottom trace) the same as above but in the presence of $ONOO^-$ (200 μM). Except for the mixture of standards, the signal intensities of the minor products (at the retention time >12 min) were multiplied by 20.

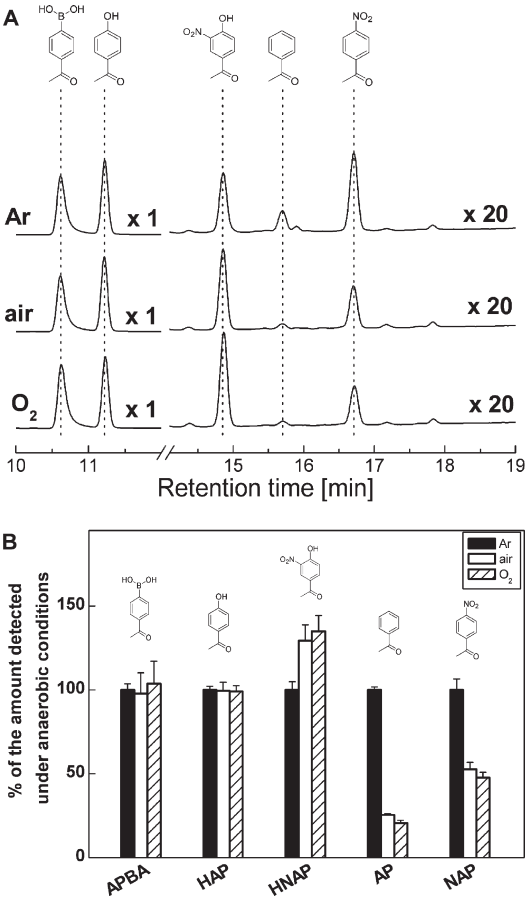

Figure 7. Effect of oxygen on products formed from the reaction between acetylphenylboronic acid and $ONOO^-$. (A) (Upper trace) Incubation mixtures containing 250 μM APBA in argon-purged phosphate buffer (pH 7.4, 50 mM) containing DTPA (100 μM) and $ONOO^-$ (200 μM), (middle trace) the same as above except under aerated conditions, and (bottom trace) the same as the upper trace except that phosphate buffer was purged with oxygen. APBA, HAP, and the minor oxidation products HNAP, AP, and NAP were detected using HPLC/UV detection at 252 nm. The signal intensities of the minor products (at the retention time >12 min) were multiplied by 20. (B) Comparison of the amount of APBA and its oxidation products in the mixtures obtained at different oxygen concentrations. The values detected under anaerobic conditions have been taken as 100%.

whose formation is easily monitored at 735 nm (ε = 1.6 × 10^4 $M^{-1}cm^{-1}$). Oxidants formed in the boronic acid/peroxynitrite reaction that can potentially oxidize ABTS to its radical cation, $ABTS^{\bullet+}$, include the $PhO_2^{\bullet}$, $PhO^{\bullet}$, and $^{\bullet}NO_2$ radicals.[27−30,33,34] The addition of ABTS caused an inhibition in the formation of HNAP without any apparent change in the yield of other radical-derived products. Similar effects were observed in the presence of tyrosine (2 mM), although small amounts of HNAP were still present (Figure 8).

The use of biologically relevant reductants (GSH, NADH, and ascorbic acid) showed a trend (Figure 9) similar to that seen with the hydrogen atom donors described above (Figure 8). Acetophenone formation was significantly enhanced in the presence of GSH and NADH (which can act as hydrogen atom donors). The inhibitory effects of ascorbic acid, tyrosine, and ABTS on the yield of HNAP can be attributed to the scavenging of phenylperoxyl and/or phenoxyl radicals, and not phenyl radicals, as there was no increase in the yield of AP (Figures 8 and 9). The lack or only a modest inhibition of NAP formation by the radical scavengers may be rationalized in terms of a rapid recombination of $Ph^{\bullet}$ and $^{\bullet}NO_2$ radicals within the solvent cage. Scheme 2 summarizes the sequence of the reactions leading to product formation in the absence of radical scavengers.

We applied several strategies to estimate the yield of the radical pairs $PhB(OH)_2O^{\bullet-}\cdots{}^{\bullet}NO_2$ formed from the homolytic cleavage of the peroxide (O−O) bond of the APBA/$ONOO^-$ adduct. We used ABTS oxidation to estimate the amount of radical pairs formed. In the presence of ABTS, the amount of $ABTS^{\bullet+}$ reflects the sum of phenyl radical and nitrogen dioxide radical concentrations. Thus, the amount of radical pairs ($PhB(OH)_2O^{\bullet-}\cdots{}^{\bullet}NO_2$) as precursors of ABTS oxidants is two times lower than the amount of $ABTS^{\bullet+}$ detected. In the case of NAP, the amount of the product directly reflects the amount of the radical pair precursors. On the basis of the concentrations of $ABTS^{\bullet+}$ (∼10−11 μM/100 μM $ONOO^-$) and of NAP (∼1−1.5 μM/100 μM $ONOO^-$), we estimated the yield of the $PhB(OH)_2O^{\bullet-}\cdots{}^{\bullet}NO_2$ radical pair to be ca. 6 μM/100 μM $ONOO^-$. The second approach to estimate the amount of radical pairs was based on quantitative analysis of the MNP-phenyl radical spin adduct (using Tempol as a standard), which indicated the yield of the MNP-phenyl radical adduct to be 4.3 μM/100 μM $ONOO^-$. This combined with the amount of HNAP and NAP detected in the presence of MNP (Supporting Information, Figure S2), indicated the total yield of phenyl radicals to be ca. 5.5 μM/100 μM $ONOO^-$. Another approach used was based on the quantitative analysis of nitration and oxidation of tyrosine induced by the radical byproduct. On the basis of the yield of nitrotyrosine (3 μM/100 μM $ONOO^-$) and

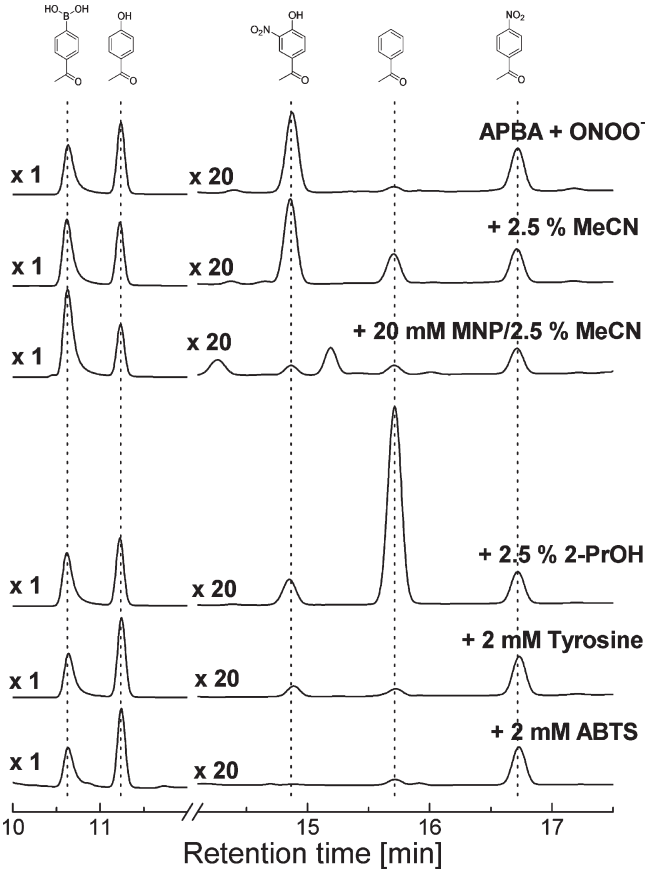

Figure 8. Effects of radical scavengers on products formed from the reaction between acetylphenylboronic acid and $ONOO^-$. HPLC chromatograms of the products of reaction between APBA and $ONOO^-$ alone and in the presence of various radical scavengers, MeCN, acetonitrile; MNP, 2-methyl-2-nitrosopropane; 2-PrOH, 2-propanol; L-tyrosine; and ABTS, 2,2′- azino-bis(3-ethylbenzothiazoline-6-sulfonic acid) diammonium salt are shown. Incubation mixtures consisted of 250 μM APBA in phosphate buffer (pH 7.4, 100 mM) containing DTPA (10 μM) and $ONOO^-$ (200 μM). APBA, HAP, and the minor oxidation products HNAP, AP, and NAP were detected using HPLC/UV detection at 252 nm. The signal intensities of the minor products (at the retention time >12 min) were multiplied by 20.

dityrosine (1.9 μM/100 μM $ONOO^-$), we estimated the yield of radical pairs being precursors of tyrosine modification as 4.9 μM/100 μM $ONOO^-$. Under these conditions, we were still able to detect HNAP, AP, and NAP with the total amounts indicative of 1.5 μM of radical pairs/100 μM $ONOO^-$ (Supporting Information, Figure S2). Thus, in the presence of tyrosine we estimated the yield of radical pairs as 6.4%. The results on the tyrosine nitration/oxidation by peroxynitrite in the presence of boronates clearly indicate the possibility of using boronic compounds as protective agents against $ONOO^-$-induced modification of intracellular components. The other approach to estimate the amount of radical pairs, based on the reduction of phenyl radicals by 2-propanol to AP, provided the yield of phenyl radicals as 8.6 μM/100 μM $ONOO^-$, from the yield of AP (8.0 μM/100 μM $ONOO^-$) and NAP (0.6 μM/100 μM $ONOO^-$, Supporting Information, Figure S2). Taken together, using four different approaches, the yield of radical pairs was estimated to lie between 5 and 9 μM/100 μM $ONOO^-$ for the reaction between APBA and $ONOO^-$.

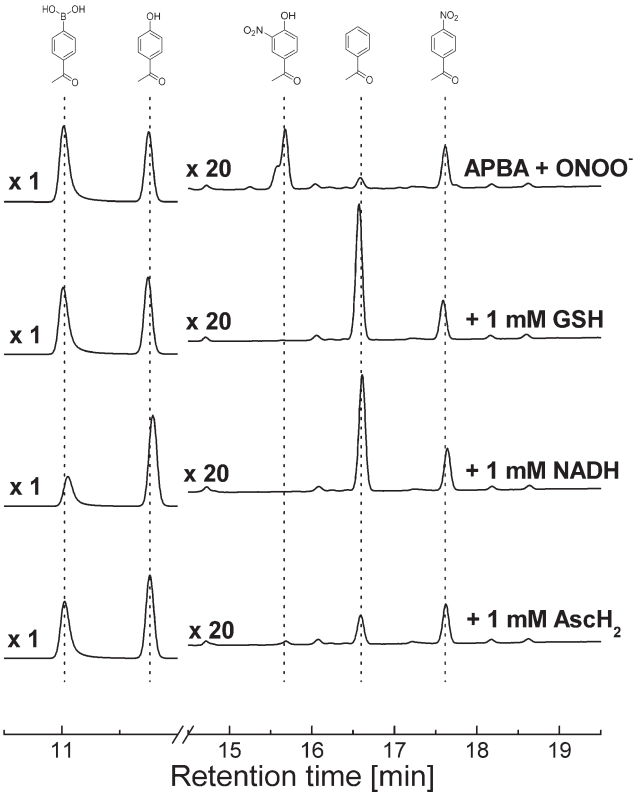

Figure 9. Effects of reductants on products formed from the reaction between acetylphenylboronic acid and $ONOO^-$. HPLC chromatograms of the reaction mixtures containing APBA and $ONOO^-$ in the presence of GSH, NADH, and ascorbic acid ($AscH_2$). Incubation mixtures contained 250 μM APBA in phosphate buffer (pH 7.4, 50 mM) containing DTPA (100 μM) and $ONOO^-$ (200 μM). APBA, HAP, and the minor oxidation products HNAP, AP, and NAP were detected using HPLC/UV detection at 252 nm. The signal intensities of the minor products (at the retention time >12 min) were multiplied by 20.

Quantum-Mechanical Studies. The DFT calculations were performed to characterize the structures of the key intermediates of the radical pathway of boronate reaction with peroxynitrite [i.e., $PhB(OH)_2O^{\bullet-}$ radical anion]. To estimate the possible role of the surrounding solvent in the postulated radical anion fragmentation, we considered a model with one water molecule explicitly included to answer the question, is the fragmentation of $PhB(OH)_2O^{\bullet-}$ preceded by protonation of the $B(OH)_2O$ part of the radical anion, and if so, does it facilitate the fragmentation? To this end, we modeled the B−C bond breaking reaction using an expanded model by adding one explicit water molecule. In both cases, we assumed the radical anion $PhB(OH)_2O^{\bullet-}$ formed upon the homolytic O−O bond cleavage undergoes further fragmentation resulting in phenyl radical ($Ph^{\bullet}$) formation. Starting from the optimized structure either of the $PhB(OH)_2O^{\bullet-}$ radical anion or its complex with explicit water molecule, we computed the potential energy surface. During optimization of the geometry of the $PhB(OH)_3^{\bullet}$ radical (the fully protonated form of $PhB(OH)_2O^{\bullet-}$), we observed the spontaneous fragmentation of the intermediate radical to the phenyl radical $Ph^{\bullet}$ and the $B(OH)_3$. This again supports the proposed mechanism of phenyl radical formation during the reaction of boronates with peroxynitrite. According to the PCM/M06-2X/6-31+G(d,p) calculations, the activation energy for the boron−carbon (B−C) bond cleavage in the $PhB(OH)_2O^{\bullet-}$ radical anion and its model with one water

Scheme 2. Sequence of the Reactions Leading to the Products (the Major Pathway Shown in Blue and the Minor Pathway in Green) during the Oxidation of Boronates by Peroxynitrite (Under Aerobic Conditions and in the Absence of Radical Scavengers)

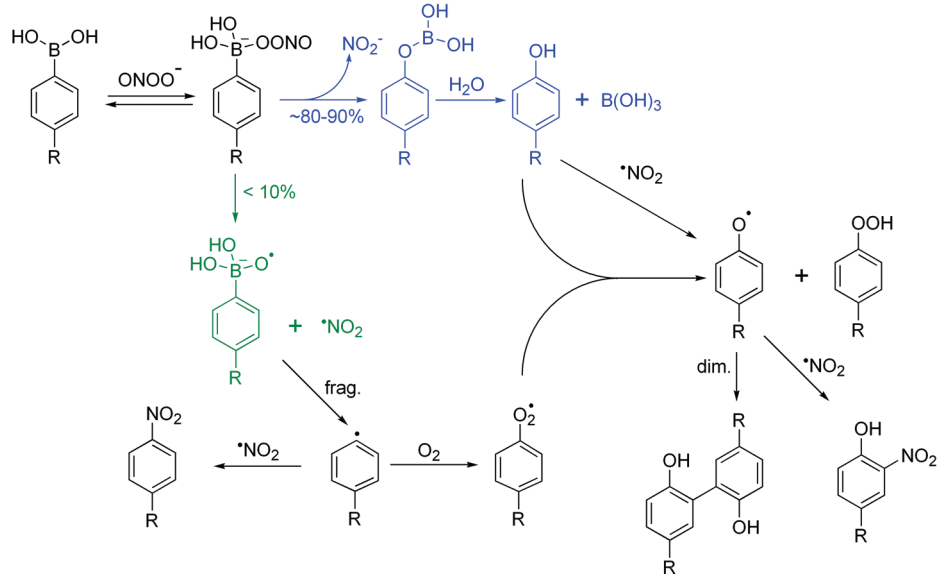

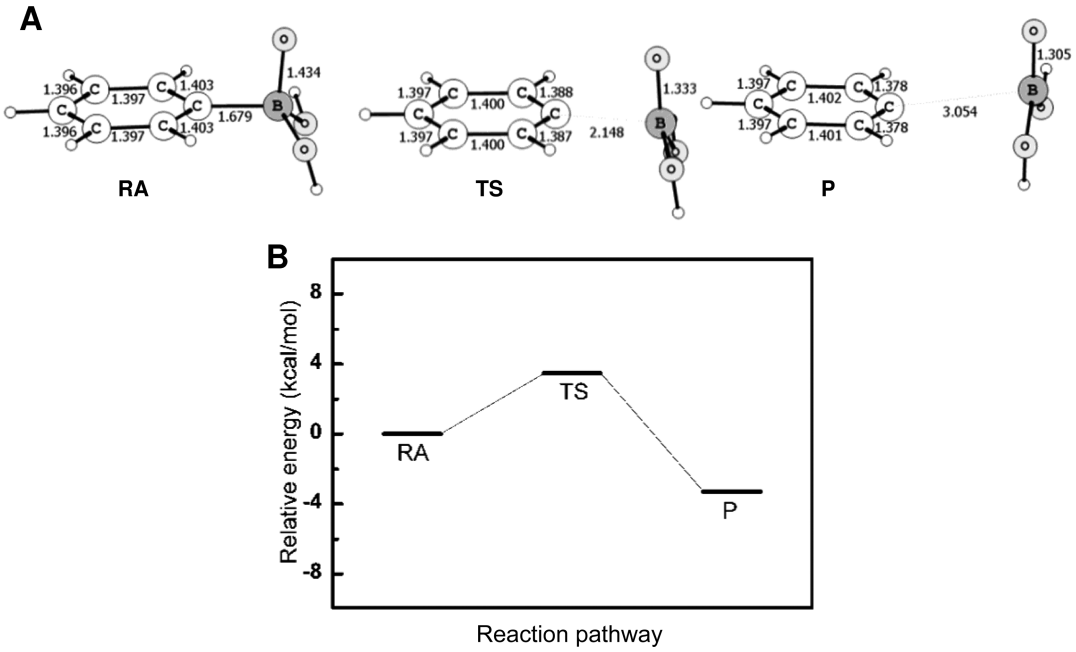

Figure 10. Fragmentation of the $PhB(OH)_2O^{\bullet-}$ radical anion. (A) PCM/M06-2X/6-31+G(d,p)-optimized structure of the $PhB(OH)_2O^{\bullet-}$ radical anion (RA), the structure of the transition state (TS) of its fragmentation reaction, and the structure of the fragmentation products (P). (B) PCM/M06-2X/6-31+G(d,p)-computed energy profile of the fragmentation reaction of the $PhB(OH)_2O^{\bullet-}$ radical anion.

molecule is only 3.5 and 4.3 kcal/mol, respectively. This suggests the possibility of fast and spontaneous fragmentation of that radical anion after its formation. On the basis of the activation energies obtained for the boron−carbon bond cleavage, it is evident that adding an explicit water molecule does not facilitate $PhB(OH)_2O^{\bullet-}$ radical anion fragmentation. Analysis of the partial atomic charges and the spin densities obtained with the APT scheme[35] clearly indicates that the majority of the radical character in the $PhB(OH)_2O^{\bullet-}$ radical anion is located on the $O^{\bullet-}$ oxygen atom, whereas in the transition state, it is carried by the carbon atom of the phenyl ring being attached to boron. Both models, with and without water assistance, resulted in a very similar distribution of partial charges and spin densities. Upon further elongation of the B−C bond, the spin density is shifted toward the phenyl ring carbon atom, while the $B(OH)_2O$ moiety retained the anionic character (Tables S1 and S2 in Supporting Information). Figure 10A shows the computed structures of the $PhB(OH)_2O^{\bullet-}$ radical anion, the transition state, and the fragmentation products. Figure 10B shows the energy profile of the $PhB(OH)_2O^{\bullet-}$ radical anion fragmentation pathway.

dx.doi.org/10.1021/tx100439a |*Chem. Res. Toxicol.* 2011, 24, 687–697

DISCUSSION

Previously, we reported that $ONOO^-$ reacts with aryl boronates nearly a million times faster than H_2O_2 and two hundred times faster than HOCl.[6] As demonstrated earlier,[6] both H_2O_2 and HOCl react with boronates directly and stoichiometrically, yielding a single major phenolic product close to 100% yield. In contrast, $ONOO^-$ reacted with boronates to form the same product, but with an 80−85% yield. Spin-trapping experiments with aryl boronates and H_2O_2 or HOCl did not reveal any radical intermediates (data not shown), consistent with the proposal that 100% of boronate is converted to 100% phenol in a two-electron oxidation/reduction process. With $ONOO^-$ dependent oxidation of boronates, however, radical intermediates were detected, leading to the formation of minor products (<15%).

Recently, we reported that the boronate-based fluorogenic probe (i.e., coumarin-7-boronic acid) was oxidized to 7-hydroxycoumarin as the predominant product in the presence of varying fluxes of $O_2^{\bullet-}$ and $^{\bullet}NO$.[7] At constant flux of $O_2^{\bullet-}$ and with increasing $^{\bullet}NO$ flux, product formation increased linearly with the maximum yield of the product occurring at a 1:1 ratio of $O_2^{\bullet-}$ and $^{\bullet}NO$ fluxes, and began to plateau at higher $^{\bullet}NO$ fluxes. In this study, we observed that the EPR signal intensities of radical adducts formed from trapping of the phenyl radicals (with both MNP and DEPMPO) also increased with the maximum yield occurring at nearly 1:1 ratio between the boronate and $ONOO^-$. These results further reiterate the proposal that both the major and minor products are formed from the same boronate/$ONOO^-$ anion adduct (Scheme 2).

The formation of phenyl radicals can be rationalized by the reaction mechanism presented in Scheme 2. We propose that the initial reaction involves the nucleophilic addition of $ONOO^-$ to the electrophilic boron atom of the boronate moiety with the formation of an anionic adduct, and the subsequent heterolytic or homolytic cleavage at the O−O bond giving the phenol and nitrite (the major, nonradical pathway), or a caged radical pair $PhB(OH)_2O^{\bullet-}\cdots\cdots{}^{\bullet}NO_2$ (the minor, radical pathway). The phenyl radical can be subsequently formed via the fragmentation of the $PhB(OH)_2O^{\bullet-}$ radical anion. According to the DFT quantum mechanical calculations, the dissociation of the $PhB(OH)_3^{\bullet}$ radical (protonated form of the $PhB(OH)_2O^{\bullet-}$ radical anion) is barrierless, and the computed energy barrier for the decomposition of $PhB(OH)_2O^{\bullet-}$ radical anion leading to the formation of phenyl radical is very low (3−4 kcal/mol), which strongly indicates the possibility of a very fast and spontaneous dissociation of that radical anion in aqueous media at room temperature. It is likely that other factors (e.g., steric hindrance and electronic effects of substituents) could alter the stability of the intermediate and the mechanism of decomposition.

In this study, we provide evidence for the formation of radical intermediates during the reaction between boronates and $ONOO^-$. The EPR spin-trapping results indicate that the yield of the DEPMPO-phenyl radical spin adduct is ca. 4%, whereas the total yield of the radical pairs formed is estimated to be ca. 5−10%. Under aerobic conditions, phenyl radicals formed via the homolytic cleavage of the O−O bond in the peroxynitrite/boronate adduct undergo a rapid reaction with the molecular oxygen, generating a highly oxidizing phenylperoxyl radical. Phenylperoxyl radicals can rapidly react with phenols, forming phenoxyl radicals and products derived from them. The inhibitory effects of phenyl radical scavengers on nitrophenol formation suggest that the phenoxyl radical is formed as the secondary species from the primary phenyl radical.

It is conceivable that the minor radical pathway derived from selected boronates may also be used in cells to further substantiate the formation of peroxynitrite because other oxidants (H_2O_2 and HOCl) do not give rise to free radical intermediates, and reactive nitrogen species such as $^{\bullet}NO_2$ do not react with boronates as does $ONOO^-$. Therefore, one can potentially use the EPR spin-trapping assay to independently confirm the formation of $ONOO^-$ in cellular systems. A thorough understanding of the reaction mechanism between boronate and peroxynitrite is toxicologically relevant because aromatic boronates and other boronate containing compounds may be used to mitigate peroxynitrite-mediated cytotoxicity.

ASSOCIATED CONTENT

Supporting Information. The results of kinetic analysis of the reaction between coumarin boronate and the DEPMPO-superoxide adduct (Figure S1), quantitative data on the yield of the products of the reaction between APBA and $ONOO^-$ in the absence and presence of radical scavengers (Figure S2), as well as the optimized geometries of all stationary points, the calculated spin and charge distribution (Tables S1 and S2), and complete ref 16 (G09). This material is available free of charge via the Internet at http://pubs.acs.org.

AUTHOR INFORMATION

Corresponding Author

*Department of Biophysics, Medical College of Wisconsin, 8701 Watertown Plank Road, Milwaukee, WI 53226. Tel: 414-456-4000. Fax: 414-456-6512. E-mail: balarama@mcw.edu.

Notes

IUPAC-recommended names for peroxynitrite anion, peroxynitrous acid, and nitric oxide are oxoperoxynitrate(−1), hydrogen oxoperoxynitrate, and nitrogen monoxide, respectively.

Funding Sources

This work was performed with the help of a grant funded by the NHLBI (R01 HL063119) awarded to B.K. A.S. was supported by a grant from the Foundation for Polish Science (FNP) within the "Homing Plus" program supported by the European Union within European Regional Development Fund, through the Innovative Economy program.

ACKNOWLEDGMENT

Access to supercomputing facilities at Cyfronet (Poland) is gratefully acknowledged.

DEDICATION

This work is dedicated to the memory of Dr. Colin Chignell. B.K. is deeply grateful for the opportunity to be involved in a photochemistry spin-trapping collaboration with Dr. Chignell when he was a visiting fellow in the Laboratory of Pharmacology at the National Institute of Environmental Health Sciences, Research Triangle Park, NC.

ABBREVIATIONS

2-PrOH, 2-propanol; ABTS, 2,2′-azino-bis(3-ethylbenzothiazoline-6-sulfonate); AP, acetophenone; APBA, 4-acetylphenylboronic acid; DEPMPO, 5-diethoxyphosphoryl-5-methyl-1-pyrroline-*N*-oxide; $AscH_2$, ascorbic acid; DTPA, diethylenetriaminepentaacetic

acid; DFT, density functional theory; FBA, phenylalanine-4-boronic acid; HAP, 4-hydroxyacetophenone; HNAP, 4-hydroxy-3-nitroacetophenone; MeCN, acetonitrile; MNP, 2-methyl-2-nitrosopropane; NAP, 4-nitroacetophenone; $^{\bullet}NO$, nitric oxide; $^{\bullet}NO_2$, nitrogen dioxide; $O_2^{\bullet-}$, superoxide radical anion; $ONOO^-$/ONOOH, peroxynitrite; PAPA-NONOate, (*Z*)-1-[*N*-(3-ammoniopropyl)-*N*-(*n*-propyl)amino]diazen-1-ium-1,2-diolate; $Ph^{\bullet}$, phenyl radical; $PhO^{\bullet}$, phenoxyl radical; $PhO_2^{\bullet}$, phenylperoxyl radical; SOD, superoxide dismutase; Tempol, 4-hydroxy-2,2,6,6-tetramethylpiperidine-1-oxyl; TFA, trifluoroacetic acid; X, xanthine; XO, xanthine oxidase.

REFERENCES

(1) Beckman, J. S., Beckman, T. W., Chen, J., Marshall, P. A., and Freeman, B. A. (1990) Apparent hydroxyl radical production by peroxynitrite: implications for endothelial injury from nitric oxide and superoxide. *Proc. Natl. Acad. Sci. U.S.A. 87*, 1620–1624.

(2) Czapski, G., and Goldstein, S. (1995) The role of the reactions of NO with superoxide and oxygen in biological systems: a kinetic approach. *Free Radical Biol. Med. 19*, 785–794.

(3) Ferrer-Sueta, G., and Radi, R. (2009) Chemical biology of peroxynitrite: kinetics, diffusion, and radicals. *ACS Chem. Biol. 4*, 161–177.

(4) Pacher, P., Beckman, J. S., and Liaudet, L. (2007) Nitric oxide and peroxynitrite in health and disease. *Physiol. Rev. 87*, 315–424.

(5) Radi, R. (2009) Peroxynitrite and reactive nitrogen species: the contribution of ABB in two decades of research. *Arch. Biochem. Biophys. 484*, 111–113.

(6) Sikora, A., Zielonka, J., Lopez, M., Joseph, J., and Kalyanaraman, B. (2009) Direct oxidation of boronates by peroxynitrite: mechanism and implications in fluorescence imaging of peroxynitrite. *Free Radical Biol. Med. 47*, 1401–1407.

(7) Zielonka, J., Sikora, A., Joseph, J., and Kalyanaraman, B. (2010) Peroxynitrite is the major species formed from different flux ratios of co-generated nitric oxide and superoxide: direct reaction with boronate-based fluorescent probe. *J. Biol. Chem. 285*, 14210–14216.

(8) Miller, E. W., Tulyathan, O., Isacoff, E. Y., and Chang, C. J. (2007) Molecular imaging of hydrogen peroxide produced for cell signaling. *Nat. Chem. Biol. 3*, 263–267.

(9) Zhao, W. (2009) Lighting up H2O2: the molecule that is a "necessary evil" in the cell. *Angew. Chem., Int. Ed. 48*, 3022–3024.

(10) Mason, R. P., and Chignell, C. F. (1981) Free radicals in pharmacology and toxicology: selected topics. *Pharmacol. Rev. 33*, 189–211.

(11) Frejaville, C., Karoui, H., Tuccio, B., Le Moigne, F., Culcasi, M., Pietri, S., Lauricella, R., and Tordo, P. (1995) DEPMPO: A new efficient phophorylated nitrone for the in vitro and in vivo spin trapping of oxygen-centered radicals. *J. Med. Chem. 38*, 258–265.

(12) Kissner, R., Beckman, J. S., and Koppenol, W. H. (1999) Peroxynitrite studied by stopped-flow spectroscopy. *Methods Enzymol. 301*, 342–352.

(13) Goss, P. A. S., Hogg, N., and Kalyanaraman, B. (1997) The effect of nitric oxide release rates on the oxidation of human low density lipoprotein. *J. Biol. Chem. 272*, 21647–21653.

(14) Hrabie, J. A., Klose, J. R., Wink, D. A., and Keefer, L. K. (1993) New nitric oxide-releasing zwitterions derived from polyamines. *J. Org. Chem. 58*, 1472–1476.

(15) Massey, V. (1959) The microestimation of succinate and the extinction coefficient of cytochrome c. *Biochim. Biophys. Acta 34*, 255–256.

(16) Frisch, M. J., et al. (2009) *Gaussian 09*, revision A.02, Gaussian, Inc., Wallingford CT.

(17) Zhao, Y., Schultz, N. E., and Truhlar, D. G. (2006) Design of density functionals by combining the method of constraint satisfaction with parametrization for thermochemistry, thermochemical kinetics, and noncovalent interactions. *J. Chem. Theory Comput. 2*, 364–382.

(18) Zhao, Y., and Truhlar, D. G. (2008) Density functionals with broad applicability in chemistry. *Acc. Chem. Res. 41*, 157–167.

(19) Hariharan, P. C., and Pople, J. A. (1973) The influence of polarization functions on molecular orbital hydrogenation energies. *Theor. Chim. Acta 28*, 213–222.

(20) Francl, M. M., Pietro, W. J., Hehre, W. J., Binkley, J. S., Gordon, M. S., DeFrees, D. J., and Pople, J. A. (1982) Self-consistent molecular orbital methods. XXIII. A polarization-type basis set for second-row elements. *J. Chem. Phys. 77*, 3654–3665.

(21) Miertus, S., Scrocco, E., and Tomasi, J. (1981) Electrostatic interaction of a solute with a continuum. A direct utilizaion of ab initio molecular potentials for the prevision of solvent effects. *Chem. Phys. 55*, 117–129.

(22) Pople, J. A., and Nesbet, R. K. (1954) Self-consistent orbitals for radicals. *J. Chem. Phys. 22*, 571–572.

(23) Chignell, C. F., and Sik, R. H. (1989) Spectroscopic studies of cutaneous photosensitizing agents--XIV. The spin trapping of free radicals formed during the photolysis of halogenated salicylanilide antibacterial agents. *Photochem. Photobiol. 50*, 287–295.

(24) Karoui, H., Hogg, N., Fréjaville, C., Tordo, P., and Kalyanaraman, B. (1996) Characterization of sulfur-centered radical intermediates formed during the oxidation of thiols and sulfite by peroxynitrite. ESR-spin trapping and oxygen uptake studies. *J. Biol. Chem. 271*, 6000–6009.

(25) Vasquez-Vivar, J., Kalyanaraman, B., Martasek, P., Hogg, N., Masters, B. S., Karoui, H., Tordo, P., and Pritchard, K. A., Jr. (1998) Superoxide generation by endothelial nitric oxide synthase: the influence of cofactors. *Proc. Natl. Acad. Sci. U.S.A. 95*, 9220–9225.

(26) Fang, X., Mertens, R., and von Sonntag, C. (1995) Pulse radiolysis of aryl bromides in aqueous solutions: some properties of aryl and arylperoxyl radicals. *J. Chem. Soc., Perkin Trans. 2*, 1033–1036.

(27) Khaikin, G. I., Alfassi, Z. B., and Neta, P. (1995) Formation and reactions of halogenated phenylperoxyl radicals in aqueous alcohol solutions. *J. Phys. Chem. 99*, 11447–11451.

(28) Khaikin, G. I., Alfassi, Z. B., and Neta, P. (1995) Inter- and intramolecular redox reactions of substituted phenylperoxyl radicals in aqueous solutions. *J. Phys. Chem. 99*, 16722–16726.

(29) Alfassi, Z. B., Khaikin, G. I., and Neta, P. (1995) Arylperoxyl radicals. Formation, absorption spectra, and reactivity in aqueous alcohol solutions. *J. Phys. Chem. 99*, 265–268.

(30) Alfassi, Z. B., Marguet, S., and Neta, P. (1994) Formation and reactivity of phenylperoxyl radicals in aqueous solutions. *J. Phys. Chem. 98*, 8019–8023.

(31) Draganic, I., Draganic, Z., Petkovic, Lj., and Nikolic, A. (1973) Radiation chemistry of aqueous solutions of simple RCN [hydrogen or alkyl cyanide] compounds. *J. Am. Chem. Soc. 95*, 7193–7199.

(32) Madhavan, V., Schuler, R. H., and Fessenden, R. W. (1978) Absolute rate constants for reactions of phenyl radicals. *J. Am. Chem. Soc. 100*, 888–893.

(33) Neta, P., and Grodkowski, J. (2005) Rate constants for reactions of phenoxyl radicals in solution. *J. Phys. Chem. Ref. Data 34*, 109–199.

(34) Forni, L. G., Mora-Arellano, V. O., Packer, J. E., and Willson, R. L. (1986) Nitrogen dioxide and related free radicals: electron-transfer reactions with organic compounds in solutions containing nitrite or nitrate. *J. Chem. Soc., Perkin Trans. 2*, 1–6.

(35) Cioslowski, J. (1989) A new population analysis based on atomic polar tensors. *J. Am. Chem. Soc. 111*, 8333–8336.

Supporting Information

We estimated the rate constant of the reaction between coumarin boronate and DEPMPO-superoxide adduct (DEPMPO-$^{\bullet}$OOH) by monitoring the formation of a highly fluorescent product, 7-hydroxycoumarin. The DEPMPO-OOH adduct was generated in incubations containing xanthine (X, 200 µM), xanthine oxidase (XO, generating a flux of $O_2^{\bullet-}$ of 6 µM/min), DEPMPO (20 mM) and DTPA (100 µM) in a phosphate buffer (50 mM, pH 7.4). After a 10 min incubation, the formation of DEPMPO-$^{\bullet}$OOH spin adduct was inhibited by adding SOD (0.05 mg/ml). Following the addition of CBE to the reaction mixture, the formation of COH was measured by monitoring the fluorescence intensity (excitation at 332 nm, emission at 450 nm) and the pseudo-first order rate constant was determined. The second order rate constant of that reaction calculated from the dependence of the pseudo-first order rate constants on CBE concentrations (see Figure S1) was *ca*. 39 $M^{-1}s^{-1}$. The quantitative data on the yield of the products of the reaction of APBA with $ONOO^-$ in the absence and presence of radical scavengers/H-atom donors are presented in Supporting Information, Figure S2. These materials also include the optimized geometries of all stationary points, the calculated spin and charge distribution (Tables S1 and S2) as well as a complete reference (*16*) (G09).

Supporting Information - Tables

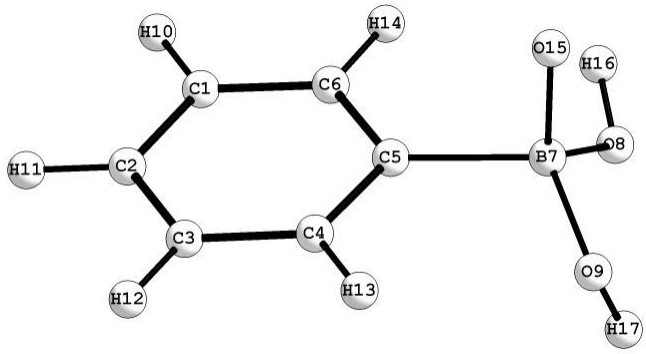

Table S1. PCM/M06-2X/6-31+G(d,p) computed APT atomic charges, and spin densities of $PhB(OH)_2O^{\bullet-}$ radical anion (RA), transition state of its fragmentation (carbon-boron bond cleavage) (TS), and the products of fragmentation process (P).

	RA		TS		P	
	CHARGES	SPIN DENSITIES	CHARGES	SPIN DENSITIES	CHARGES	SPIN DENSITIES
1 C	-0.041	-0.016	0.012	0.022	0.002	0.062
2 C	-0.102	0.046	-0.150	-0.010	-0.107	-0.043
3 C	-0.037	-0.019	0.014	0.024	0.007	0.048
4 C	-0.081	0.033	-0.191	-0.026	-0.092	-0.112
5 C	-0.272	0.106	0.440	0.706	-0.013	1.022
6 C	-0.068	0.039	-0.193	-0.035	-0.095	-0.054
7 B	1.414	-0.036	1.528	-0.030	1.887	-0.008
8 O	-1.056	0.008	-1.035	0.009	-1.091	0.007
9 O	-1.034	0.004	-1.018	0.004	-1.074	0.010
10 H	0.025	0.001	0.018	0.005	0.048	0.007
11 H	0.034	-0.002	0.044	0.001	0.059	0.002
12 H	0.023	0.001	0.017	0.006	0.048	0.007
13 H	0.045	0.000	0.075	0.015	0.095	0.023
14 H	0.013	0.000	0.046	0.015	0.083	0.022
15 O	-0.494	0.834	-1.269	0.295	-1.421	0.007
16 H	0.314	-0.001	0.329	-0.001	0.331	0.000
17 H	0.317	-0.001	0.333	-0.001	0.333	-0.001
Ph	-0.461	0.191	0.132	0.723	0.035	0.984
BA	-0.539	0.809	-1.132	0.277	-1.035	0.016

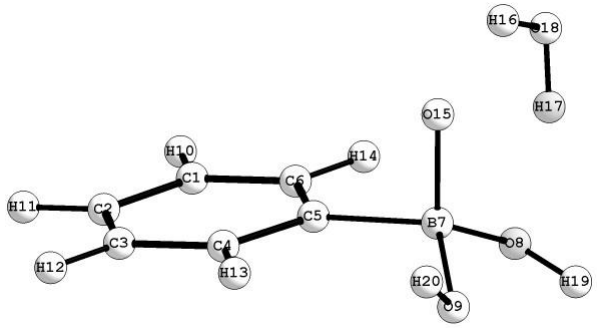

Table S2. PCM/M06-2X/6-31+G(d,p) computed APT atomic charges, and spin densities of $PhB(OH)_2O^{\bullet-}$ radical anion water complex (RA), transition state of $PhB(OH)_2O^{\bullet-}$ water-assisted fragmentation (carbon-boron bond cleavage) (TS), and the products of fragmentation process (P).

	RA		TS		P	
	CHARGES	SPIN DENSITIES	CHARGES	SPIN DENSITIES	CHARGES	SPIN DENSITIES
1 C	-0.046	-0.017	0.016	0.022	0.012	0.039
2 C	-0.089	0.051	-0.136	-0.010	-0.105	-0.042
3 C	-0.050	-0.015	0.000	0.025	-0.010	0.086
4 C	-0.051	0.030	-0.176	-0.063	-0.087	0.141
5 C	-0.274	0.078	0.405	0.704	-0.040	0.979
6 C	-0.069	0.058	-0.210	0.004	-0.129	-0.274
7 B	1.379	-0.035	1.561	-0.023	1.884	-0.003
8 O	-1.089	0.006	-1.052	0.013	-1.081	0.005
9 O	-1.036	0.005	-1.041	0.006	-1.069	0.008
10 H	0.024	0.001	0.021	0.005	0.047	0.007
11 H	0.034	-0.002	0.046	0.001	0.060	0.003
12 H	0.027	0.001	0.022	0.006	0.050	0.007
13 H	0.025	0.000	0.079	0.015	0.084	0.020
14 H	0.049	0.000	0.091	0.015	0.171	0.025
15 O	-0.532	0.840	-1.360	0.284	-1.500	-0.002
16 H	0.461	-0.002	0.721	-0.004	0.785	0.000
17 H	0.514	0.000	0.365	0.000	0.341	0.000
18 O	-0.916	0.002	-1.014	0.002	-1.082	0.000
19 H	0.318	0.001	0.333	-0.001	0.331	0.000
20 H	0.322	0.000	0.330	-0.001	0.338	0.000
Ph	-0.421	0.185	0.156	0.723	0.052	0.992
BA	-0.638	0.815	-1.229	0.279	-1.096	0.008
H2O	0.059	0.000	0.073	-0.002	0.045	0.000

Supporting Information - Figure Legends

Figure S1. Determination of the rate constant of the reaction between DEPMPO-$^{\bullet}$OOH spin adduct and CBE. Xanthine (X, 200 μM), xanthine oxidase (XO, generating a flux of $O_2^{\bullet-}$ of 4 μM/min) and DEPMPO (20 mM) were pre-incubated in a phosphate buffer (50 mM, pH 7.4) containing DTPA (100 μM). Ten minutes after the reaction, the accumulation of the DEPMPO-$^{\bullet}$OOH adduct was stopped by adding SOD (8 μg/ml). After the addition of CBE, the formation of COH was followed by monitoring the fluorescence intensity (excitation at 332 nm, emission at 450 nm) and the pseudo-first order rate constant was determined.

Figure S2. The effect of H-atom donors/radical scavengers on the yield of major/minor products of the reaction between APBA and $ONOO^-$. APBA (250 μM) in phosphate buffer (50 mM, pH 7.4) containing DTPA (100 μM) was reacted with $ONOO^-$ (190 ± 10 μM) in the absence and presence of radical scavengers: GSH (1 mM), NADH (1 mM), $AscH_2$ (1 mM), MeCN (2.5% by vol.), MNP (20 mM, 2.5% MeCN), 2-PrOH (2.5% by vol.), tyrosine (2 mM) and ABTS (2 mM). Error bars represent standard deviation (n = 3).

Figure S1

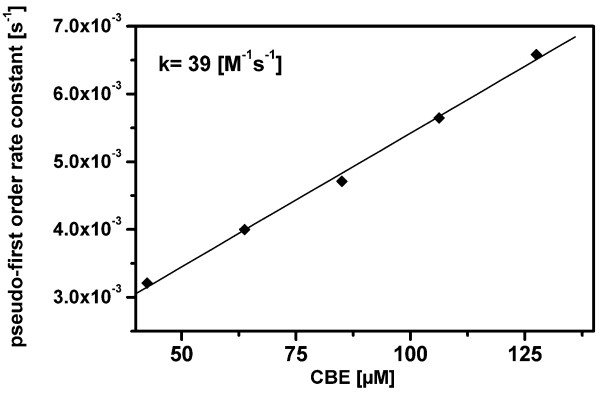
pseudo-first order rate constant [s^{-1}]
7.0x10^{-3}
6.0x10^{-3}
5.0x10^{-3}
4.0x10^{-3}
3.0x10^{-3}
k= 39 [M^{-1}s^{-1}]
50
75
100
125
CBE [µM]

Figure S2

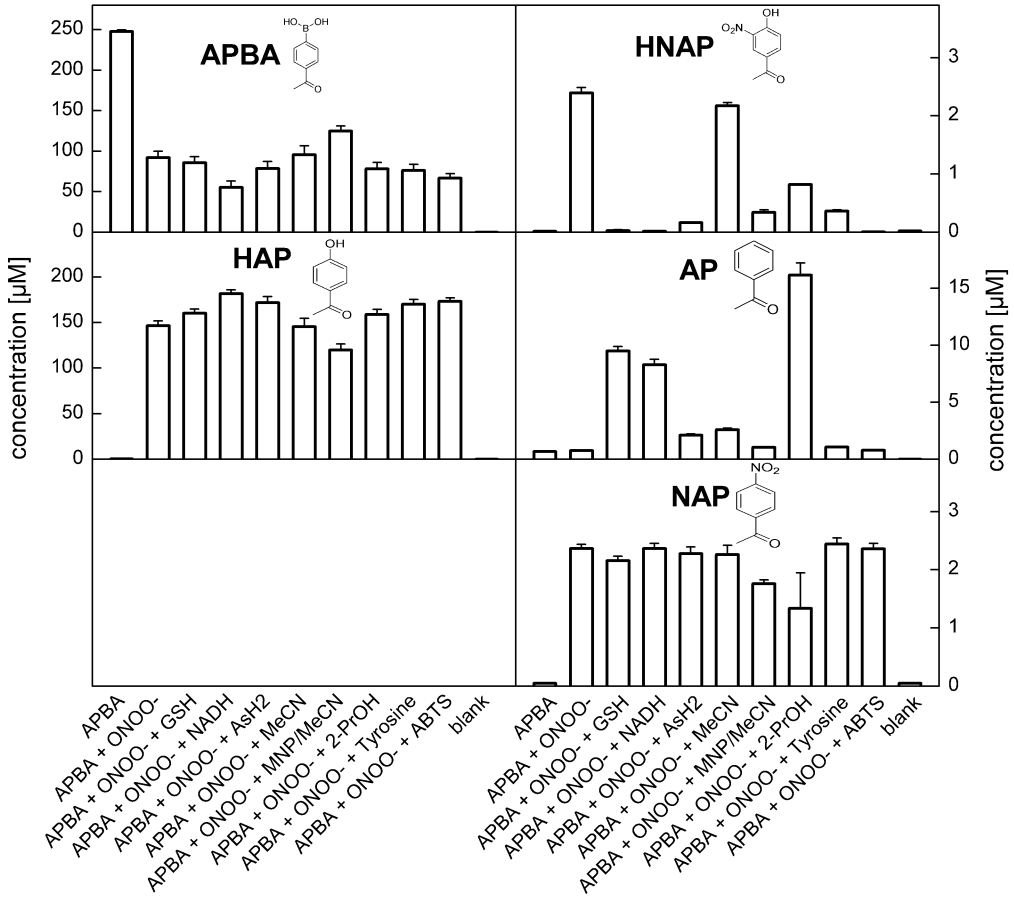
APBA
HNAP
HAP
AP
NAP
concentration [µM]
concentration [µM]
APBA
APBA + ONOO-
APBA + ONOO- + GSH
APBA + ONOO- + NADH
APBA + ONOO- + AsH2
APBA + ONOO- + MeCN
APBA + ONOO- + MNP/MeCN
APBA + ONOO- + 2-PrOH
APBA + ONOO- + Tyrosine
APBA + ONOO- + ABTS
blank

Full reference 16:

(16) Frisch, M. J., Trucks, G. W., Schlegel, H. B., Scuseria, G. E., Robb, M. A., Cheeseman, J. R., Scalmani, G., Barone, V., Mennucci, B., Petersson, G. A., Nakatsuji, H., Caricato, M., Li, X., Hratchian, H. P., Izmaylov, A. F., Bloino, J., Zheng, G., Sonnenberg, J. L., Hada, M., Ehara, M., Toyota, K., Fukuda, R., Hasegawa, J., Ishida, M., Nakajima, T., Honda, Y., Kitao, O., Nakai, H., Vreven, T., Montgomery, J. A. Jr., Peralta, J. E., Ogliaro, F., Bearpark, M., Heyd, J. J., Brothers, E., Kudin, K. N., Staroverov, V. N., Kobayashi, R., Normand, J., Raghavachari, K., Rendell, A., Burant, J. C., Iyengar, S. S., Tomasi, J., Cossi, M., Rega, N., Millam, J. M., Klene, M., Knox, J. E., Cross, J. B. Bakken, V., Adamo, C., Jaramillo, J., Gomperts, R., Stratmann, R. E., Yazyev, O., Austin, A. J., Cammi, R., Pomelli, C., Ochterski, J. W. Martin, R. L., Morokuma, K., Zakrzewski, V. G., Voth, G. A., Salvador, P., Dannenberg, J. J., Dapprich, S., Daniels, A. D., Farkas, O., Foresman, J. B., Ortiz, J. V., Cioslowski, J., and Fox, D. J. (2009) *Gaussian 09, Revision A.02*, Gaussian, Inc., Wallingford CT.

Energies and geometries of all stationary points located

and characterized in the course of this study;

Note: All structures are optimized taking into account the influence of the environment, which was modeled using the polarizable continuum solvent model (PCM) with parameters for water as implemented in Gaussian 09; energies are in hartree.

Radical Anion

-1 2

6	2.166819000	-1.196418000	-0.067101000
6	2.861713000	0.014439000	-0.087331000
6	2.150754000	1.215115000	-0.038055000
6	0.755730000	1.198063000	0.028329000
6	0.034435000	-0.004886000	0.031005000
6	0.771888000	-1.197988000	-0.000264000
5	-1.644254000	0.010603000	0.058968000
8	-2.240566000	-1.078198000	-0.738544000
8	-2.195316000	1.276381000	-0.438659000
1	2.712155000	-2.135976000	-0.102036000
1	3.946699000	0.021805000	-0.138897000
1	2.684844000	2.161827000	-0.051407000
1	0.205654000	2.135810000	0.060090000
1	0.251212000	-2.154426000	0.016831000
8	-1.757870000	-0.133995000	1.481164000
1	-2.021449000	-1.931635000	-0.352199000
1	-2.455856000	1.166121000	-1.358411000

Electronic energy= -483.405886
Sum of electronic and zero-point Energies= -483.280659
Sum of electronic and thermal Energies= -483.271006
Sum of electronic and thermal Enthalpies= -483.270062
Sum of electronic and thermal Free Energies= -483.316308

Transition State

-1 2

6	2.275169000	-1.179120000	-0.092241000
6	2.930835000	0.053704000	-0.136535000
6	2.195693000	1.238159000	-0.050976000
6	0.802008000	1.194415000	0.078972000
6	0.170854000	-0.040439000	0.106107000
6	0.882578000	-1.230023000	0.041230000
5	-1.976693000	-0.008053000	0.125912000
8	-2.335684000	-0.995861000	-0.854265000
8	-2.276341000	1.305676000	-0.350383000
1	2.847048000	-2.101480000	-0.154996000
1	4.011694000	0.090676000	-0.233727000
1	2.706357000	2.197406000	-0.084316000
1	0.218819000	2.109557000	0.139256000
1	0.373449000	-2.190299000	0.088490000
8	-1.780332000	-0.271589000	1.418113000
1	-2.184659000	-1.871182000	-0.483012000
1	-2.493206000	1.279608000	-1.288316000

Electronic energy= -483.400330
Sum of electronic and zero-point Energies= -483.275691

Sum of electronic and thermal Energies= -483.266368
Sum of electronic and thermal Enthalpies= -483.265424
Sum of electronic and thermal Free Energies= -483.311314

Phenyl Radical B(OH)2O- Pair

-1 2

6	-2.626195000	1.169858000	0.033986000
6	-3.220151000	-0.091903000	0.110872000
6	-2.439285000	-1.249409000	0.059801000
6	-1.047219000	-1.154885000	-0.069358000
6	-0.513206000	0.113696000	-0.141785000
6	-1.235251000	1.286853000	-0.095532000
5	2.521989000	-0.042927000	0.161599000
8	2.563724000	1.137902000	-0.645187000
8	2.381044000	-1.200263000	-0.653292000
1	-3.240799000	2.064604000	0.073840000
1	-4.297862000	-0.173957000	0.211462000
1	-2.910025000	-2.226485000	0.122130000
1	-0.419491000	-2.039742000	-0.108779000
1	-0.757568000	2.260295000	-0.157165000
8	2.626831000	-0.070781000	1.461665000
1	2.653368000	1.900724000	-0.065009000
1	2.277483000	-0.950931000	-1.577856000

Electronic energy= -483.411137
Sum of electronic and zero-point Energies= -483.285536
Sum of electronic and thermal Energies= -483.275080
Sum of electronic and thermal Enthalpies= -483.274136
Sum of electronic and thermal Free Energies= -483.325197

Radical Anion and Water Complex

-1 2

6	-2.084088000	1.475174000	-0.374514000
6	-3.089752000	0.575272000	-0.015393000
6	-2.750641000	-0.734389000	0.329818000
6	-1.413162000	-1.134955000	0.312560000
6	-0.389167000	-0.253341000	-0.061084000
6	-0.750284000	1.062739000	-0.386233000
5	1.195793000	-0.751901000	-0.118083000
8	1.921662000	0.034932000	-1.138271000
8	1.389668000	-2.171325000	-0.433523000
1	-2.340858000	2.497047000	-0.641282000
1	-4.128504000	0.892695000	-0.002147000
1	-3.527815000	-1.439822000	0.612008000
1	-1.163649000	-2.160328000	0.579795000
1	0.028091000	1.769975000	-0.664791000
8	1.498739000	-0.418097000	1.256271000
1	2.240546000	1.476416000	1.209640000
1	2.496051000	1.579963000	-0.245115000
8	2.613610000	2.105088000	0.570005000
1	2.640434000	-0.505600000	-1.483644000
1	1.249876000	-2.698629000	0.359169000

Electronic energy= -559.824847
Sum of electronic and zero-point Energies= -559.674128
Sum of electronic and thermal Energies= -559.661783
Sum of electronic and thermal Enthalpies= -559.660839
Sum of electronic and thermal Free Energies= -559.713435

Transition State and Water Complex

-1 2

6	2.167981000	1.405557000	0.425825000
6	3.140090000	0.458493000	0.093791000
6	2.759277000	-0.817672000	-0.326417000
6	1.402655000	-1.154415000	-0.415141000
6	0.461517000	-0.201239000	-0.060251000
6	0.809800000	1.080166000	0.337933000
5	-1.550596000	-0.788682000	0.036333000
8	-2.031440000	-0.066490000	1.182350000
8	-1.457245000	-2.208426000	0.164857000
1	2.466410000	2.399752000	0.748185000
1	4.192914000	0.716173000	0.158681000
1	3.516748000	-1.553305000	-0.584865000
1	1.092254000	-2.146202000	-0.732214000
1	0.041136000	1.809277000	0.580743000
8	-1.638429000	-0.224161000	-1.177651000
1	-2.073522000	1.319815000	-0.896111000
1	-2.469675000	2.058716000	0.371846000
8	-2.380783000	2.221454000	-0.575849000
1	-1.954422000	-0.544424000	2.013431000
1	-1.443609000	-2.520731000	1.074556000

Electronic energy= -559.818028
Sum of electronic and zero-point Energies= -559.669328
Sum of electronic and thermal Energies= -559.657105
Sum of electronic and thermal Enthalpies= -559.656161
Sum of electronic and thermal Free Energies= -559.708961

Phenyl Radical, B(OH)2O- and Water Complex

-1 2

6	2.058496000	1.407442000	-0.177933000
6	3.294644000	0.756263000	-0.167254000
6	3.366831000	-0.627256000	0.007233000
6	2.194361000	-1.378418000	0.173160000
6	1.004728000	-0.683045000	0.156203000
6	0.872749000	0.678928000	-0.012930000
5	-2.184361000	-0.717745000	-0.162849000
8	-2.024736000	-0.361164000	1.202965000
8	-2.056114000	-2.084599000	-0.502515000
1	2.012708000	2.484346000	-0.314294000
1	4.207419000	1.329801000	-0.295037000
1	4.331392000	-1.126928000	0.014497000
1	2.234732000	-2.455092000	0.308168000
1	-0.101278000	1.162959000	-0.017763000
8	-2.460008000	0.198362000	-1.063038000
1	-2.364026000	1.552082000	-0.363296000
1	-2.107266000	2.085891000	1.069467000
8	-2.266502000	2.418922000	0.178202000
1	-1.846711000	-2.666952000	0.234044000
1	-1.737144000	-1.073033000	1.782670000

Electronic energy= -559.830786
Sum of electronic and zero-point Energies= -559.680755
Sum of electronic and thermal Energies= -559.667835
Sum of electronic and thermal Enthalpies= -559.666891
Sum of electronic and thermal Free Energies= -559.723360
